 doi:10.20944/preprints202206.0287.v1

Article

The Dissipative Photochemical Origin of Life: UVC Abiogenisis of the Purines

Claudeth Hernández[1] and Karo Michaelian[2]

[1] Department of Physics, Division of Exact and Natural Sciences, Universidad de Sonora, Campus Hermosillo, México, C.P. 83067; claudeth.clarissa@gmail.com

[2] Department of Nuclear Physics and Application of Radiation, Instituto de Física, Universidad Nacional Autónoma de México, Circuito Interior de la Investigación Científica, Cuidad Universitaria, Cuidad de México, México, C.P. 04510.; karo@fisica.unam.mx

* karo@fisica.unam.mx

Abstract: We have suggested that the abiogenisis of life around the beginning of the Archean may have been an example of microscopic dissipative structuring of UVC pigments (the fundamental molecules of life) under the prevailing surface UV solar spectrum. In a previous article in this series, we have describe the non-equilibrium thermodynamics and the photochemical mechanisms which may have been involved in the dissipative structuring of the purines adenine and hypoxanthine from the common precursor molecules of HCN and water under UVC light. In this article we extend our analysis to include the production of the other two important purines, guanine and xanthine, from these same precursors. The photochemical reactions are presumed to occur within a fatty acid vesicle floating on a hot ocean surface exposed to the prevailing UV light. Reaction-diffusion equations are resolved under different environmental conditions. Significant amounts of adenine ($\sim 10^{-5}$M) and guanine ($\sim 10^{-6}$M) are obtained within only a few months at 80 °C under plausible initial concentrations of HCN and cyanogen (a photochemical product of HCN).

Keywords: origin of life; disspative structuring; non-equilibrium thermodynamics; prebiotic chemistry; abiogenisis; adenine; guanine; hypoxanthine; xanthine; purines

PACS: 05.70.Ln, 91.62.Uv, 91.62.+g, 91.62.Kt, 91.62.Np, 91.70.h, 87.14.gk, 87.14.gn, 87.15.-v, 87.16.Dg, 87.23.-n

MSC: 92C05, 92C15, 92C40, 92C45, 92D15, 80A99, 82C99

1. Introduction

Possible chemical or photochemical routes to the production of the purines, including adenine, hypoxanthine, guanine, xanthine, and 2,6-diaminopurine from common precursor molecules, have been extensively studied since the first experiments of Miller and Urey in 1953. Sources of free energy for synthesis have included; heat gradients, lightning, UV light, and shock waves. Plausible precursor molecules are HCN and water, along with the photochemical and hydrloysis products of HCN, which include formamide, amonium formate, cyanogen and cyanate [1–13]. These experiments, however, were usually carried out at alkaline pH and unrealistically large HCN concentrations (>0.1 M) because, only under these conditions, polymerization of HCN to cis-DAMN (an intermediate on route to adenine and guanine, see figure 1) prevails over hydrolysis.

From the perspective of the "Thermodynamic Dissipation Theory of the Origin of Life" [14–28], descriptions of molecular synthesis alone, however, are insufficient to describe life's vitality,

 doi:10.20944/preprints202206.0287.v1

which includes proliferation, dynamics, and evolution. The vitality of life requires instead a constant dissipation of an imposed thermodynamic potential. Of the above listed free energy sources used in synthesis experiments, only UV light would have been of sufficient intensity and continuously available throughout the Archean. Our theory therefore affirms that the fundamental molecules of life were, at their origin, microscopic dissipative structures (i.e UVC pigments) which arose "spontaneously" to dissipate the UVC solar photon spectrum [14,15,21,26].

In this paper we model the origin of life as a photochemical dissipative structuring process with reaction-diffusion occurring within a fatty acid vesicle floating at the ocean surface, permeable to the precursor molecules HCN, cyanogen, and H_2O, and under a UVC photon flux arriving at Earth's surface during the Archean (Figure 2 of Michaelian [26]). Starting from a realistic environmental HCN concentration of 6×10^{-5} M we show that adenine and guanine concentrations of 2.4×10^{-5} M and 7.6×10^{-7} M respectively, could have been obtained through such UVC photochemical dissipative structuring at 80 °C in only 60 Archean days. These purine concentrations increase or decrease by roughly an order of magnitude for each 10 °C increase or decrease in surface temperature.

2. Thermodynamics of Dissipative Structuring

We have identified the long wavelength part of the UVC region ($\sim$ 210-285 nm), plus the long wavelength part of the UVB and short wavelength part of the UVA regions ($\sim$ 310-360 nm), of the solar spectrum as the thermodynamic potential which could have driven the molecular dissipative structuring [21,26], proliferation, and evolution relevant to the origin of life. This light prevailed at Earth's surface from the Hadean, before the origin of life (soemwhere near the beginning of the Archean $\sim$ 3.9 Ga), and for perhaps as long as 1600 million years [29–31] until the formation of an ozone layer at about 2.5 Ga after natural oxygen sinks (e.g., volcanic reducing gases such as CO or H_2S and Fe^{+2}) became overwhelmed by organisms performing oxygenic photosynthesis, perhpas fertilized by volcanic phosphorus [32].

The relevance of this particular region of the solar spectrum, corresponding to the Archean atmospheric window of transparency, to the dissipative structuring of the fundamental molecules is that longer wavelengths do not contain sufficient free energy to directly break double covalent carbon bonds, while shorter wavelengths contain enough free energy to destroy carbon based molecules through successive ionization or fragmentation.

A number of empirical evidences support our dissipative structuring conjecture for the fundamental molecules of life. First, the wavelength of maximum absorption of many of these molecules coincide with the predicted window in the Archean atmosphere (see Figure 2 of Michaelian [26]). Secondly, many of the fundamental molecules of life are endowed with *peaked conical intersections* (reference [26]) giving them broad band absorption and high quantum yield for internal conversion, i.e. extremely rapid (picosecond) dissipation of the photon-induced electronic excitation energy into vibrational energy of molecular atomic coordinates, and finally into the surrounding water solvent [21,33]. The most convincing evidence of all, however, is that many photochemical routes to the synthesis of nucleic acids [34], amino acids [35], fatty acids [23], sugars [36], and other pigments [18] from common and simple precursor molecules have been identified at these wavelengths and the rate of photon dissipation within the Archean window generally increases after each incremental step on route to synthesis, a behavior strongly suggestive of dissipative structuring in the non-linear non-equilibrium regime [21,23,26]. Finally, even small changes (e.g. tautomerizations) or additions to the fundamental molecules will render inoperative these special optical properties.

The photochemistry involved in the non-equilibrium thermodynamics of dissipative structuring and proliferation of the fundamental molecules, and how this leads to the evolution of molecular concentration profiles with ever greater solar photon dissipation capacity (corresponding to increases in global entropy production) has been described in detail elsewhere (Michaelian [26]). Here we detail those most important aspects pertaining to the dissipative structuring of the purines guanine and xanthine.

 doi:10.20944/preprints202206.0287.v1

3. The Dissipative Structuring of the Purines

3.1. The Model

Cyanogen, HCN, and its hydrolysis product formamide, were first recognized by Eduard Pflüger in 1875 to be the probable precursors of life [37]. The fundamental molecules; nucleic acids, amino acids, fatty acids [36], and even simple sugars [38,39] have all been synthesized from these precursors.

HCN is found throughout the cosmos [40,41] and its production during the Hadean and Archean on Earth was probably a result of the solar Lyman alpha line (121.6 nm) photo-lysing N_2 in the upper atmosphere. The resulting radical could then attack CH or CH_2 to form HCN. Another possibility is the UV (145 nm) photolysis of CH_4 in the middle atmosphere leading to a CH^* radical attacking N_2 [42,43].

Cyanogen, NCCN or $(CN)_2$, can be generated from HCN either photochemically [44] or thermally [45]. The Lyman-α line on middle atmospheric HCN will produce, through photolysis, the CN^- radical with high quantum yield (reaction R177 table 1, Zahnle [46]) and this radical gives cyanogen after interaction with a second HCN molecule (reaction R199 of table 1 of Zahnle). Both HCN and cyanogen have been found in the atmosphere of Titan [43] where they probably derive from similar UV photochemical processes in Titan's upper or middle atmosphere.

Our proposed photochemical route to the purines from these precursors is based on the experimental data of Ferris and Orgel [34] and Sanchez et al. [6], as well as the quantum mechanical calculations of Boulanger et al. [47], and is given in figure 1.

Preprints (www.preprints.org) | NOT PEER-REVIEWED | Posted: 21 June 2022 doi:10.20944/preprints202206.0287.v1

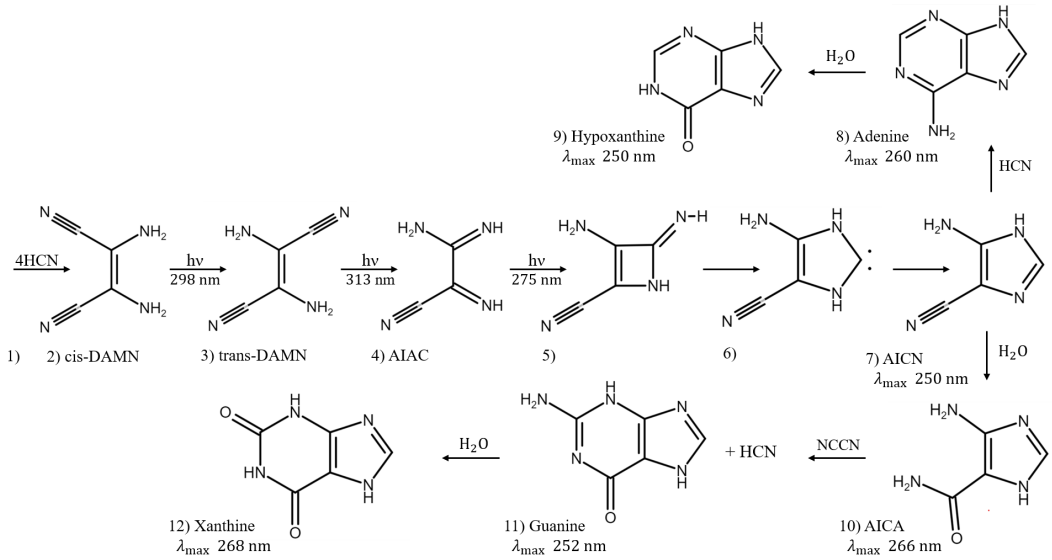

Figure 1. The photochemical synthesis of adenine and guanine from 4 molecules of hydrogen cyanide (HCN) in water, and a final HCN for adenine (as discovered by Ferris and Orgel (1966) [34,47]), and a cyanogen molecule for guanine (as discovered by Sanchez et al. [6]). Four molecules of HCN are transformed into the smallest stable oligomer (tetramer) of HCN, known as cis-2,3-diaminomaleonitrile (cis-DAMN) (2), which, under a constant UVC photon flux isomerizes into significant concentrations of trans-DAMN (3) (diaminofumaronitrile, DAFN) which may be further converted on absorbing two more UVC photons into an imidazole intermediate, 4-amino-1H-imidazole-5-carbonitrile (AICN) (7). Hot ground state thermal reactions with another HCN molecule, or its hydrolysis product formamide (or ammonium formate), leads to the purine adenine (8). Hydrolysis of adenine (8) leads to hypoxanthine (9). Hydrolysis of AICN (7) leads to AICA (10) and a hot ground state thermal reaction with a cyanogen molecule leads to guanine (11). Hydrolysis of guanine (11) leads to xanthine (12). This is a microscopic dissipative structuring process under UVC light which ends in the purines; adenine and hypoxanthine [21,26] as well as guanine and xanthine, all UVC pigments with large molar extinction coefficient at 260, 250, 252 and 268 nm respectively and with peaked conical intersections providing rapid dissipation of photons around the wavelengths of maximum intensity of the Archean surface solar UVC spectrum (figure 2 of Michaelian [26]). Adapted from Ferris and Orgel (1966) [34].

The route to guanine results from the hydrolysis of 4-aminoimidazole-5-carbonitrile (AICN) to form 2-amino-3-iminoacrylimidoyl cyanide (AICA) (step 7 to 10 of figure 1) which then combines through a thermal chemical reaction with cyanogen (NCCN) to form guanine plus a HCN molecule [6]. The reactions on route to adenine and guanine are in competition with hydrolysis and UV lysis, and these relative rates are dependent on concentrations, temperature, pH, the presence of metal ion- and organic intermediate product catalysts, as well as the wavelength dependent intensity of the incident UV spectrum. Some of these complexities have been studied by Sanchez et al. [5,6]. Very favorable comparisons of our simulated photochemical production rates to experimental data have been given in Michaelian [26] (this special issue).

In Michaelian [26] we have addressed the issue of the expected low concentration of HCN in the Archean oceans leading to a low polymerization rate of HCN with respect to its rate of hydrolysis. Traditional approaches to the origin of life have "resolved" this issue by invoking eutectic concentration to increase the solute HCN concentration to values sufficient for biasing the reactions towards polymerization [48–50]. This low temperature approach, however, reduces significantly all thermal reaction rates. Instead, we have emphasized the existence of an ocean surface microlayer of high organic concentration, 10^4 or 10^5 greater than that of bulk water (see Michaelian [26] for discussion and references). We also assume the existence of fatty acid vesicles of ~ 100 μm diameter which would allow the incident UVC light, as well as the small precursor molecules, HCN, cyanogen,

Preprints (www.preprints.org) | NOT PEER-REVIEWED | Posted: 21 June 2022 doi:10.20944/preprints202206.0287.v1

and H_2O, to permeate unimpeded the vesicle bi-layer wall (figure 2), while trapping inside the reaction products due to their larger sizes and larger dipole moments (Table 1). This allows the intermediate and product molecules, as well as the heat from UVC photon dissipation, to accumulate within the vesicle.

The existence of amphipathic fatty acid hydrocarbon chains, which through Gibb's free energy minimization spontaneously form lipid vesicles at the ocean surface, is a common assumption in origin of life scenarios [51,52]. The abiogenisis of fatty acids during the Archean could be attributed to the dissipative structuring under UVC photons of HCN and CO_2 saturated water at moderate temperatures on the ocean surface [23]. In order to maintain vesicle integrity at the high surface temperatures considered here at the beginning of the Archean of $\sim 80°C$ [53–55] these fatty acids would necessarily have been long ($\sim$ 18 C atoms) and cross linked through UVC light, which improves stability at high temperatures and over a wider range of pH values [23,56]. There is, in fact, a predominance of 16 and 18 carbon atom fatty acids in the whole Precambrian fossil record [57,58].

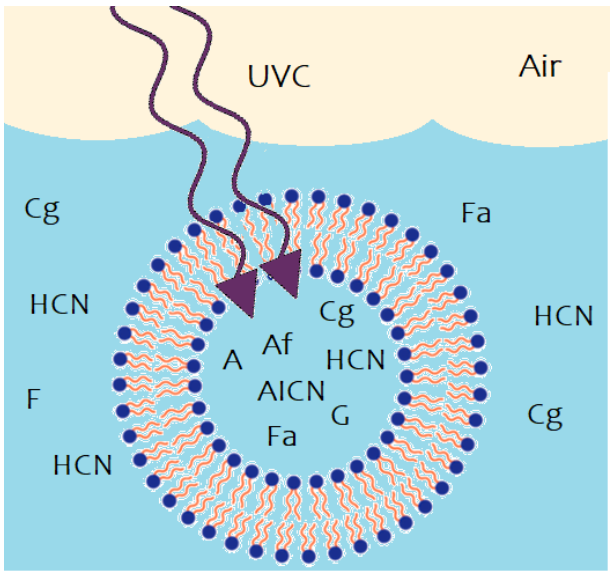

Figure 2. Fatty acid vesicle floating at the ocean surface microlayer of high organic concentration, transparent to UVC light and permeable to the small precursor molecules having small dipole moments; H_2O, HCN (H), cyanogen (Cy), and formimidic acid (Fa), but impermeable to the intermediate and final photochemical products (e.g. ammonium formate (Af), cis-DAMN, AICN, adenine (A), guanine (G)), which are larger in size and have larger dipole moments (Table 1).

In the following subsection we present a simplified out-of-equilibrium kinetic model for our 5HCN $\rightarrow$ adenine and 4HCN + H_2O + NCCN $\rightarrow$ guanine + HCN (Figure 1) photochemical reaction system occurring within a fatty acid vesicle floating within the high organic concentration microlayer of a hot ($\sim 80°C$ [53–55]) Archean ocean surface under the UV surface spectrum of figure 2 of reference [26]. The system is under a diurnal 8 hr constant flux of radiation followed by an 8 hour period of darkness during which thermal reactions proceed, but not photochemical reactions. The system is perturbed by a single patch of relatively high concentration (0.1 M) of HCN, cyanogen (Cg), and formimidic acid (Fa) (see Michaelian [26] for a description) into which our vesicle is assumed to drift only once for 2 minutes during 60 Archean days.

The kinetic equations for the above model of chemical and photochemical reactions are resolved numerically. For this perturbed non-linear reaction-diffusion system it will be shown in Section 4 that various stationary state solutions exist with spatial symmetry breaking resulting in the highest concentration of purines at the center of the vesicle. This would then facilitate a subsequent UVC polymerization of nucleobases into short oligos (of course assuming the possibility of UVC-assisted synthesis of ribose from similar precursor molecules [39] and a temperature [59]

Preprints (www.preprints.org) | NOT PEER-REVIEWED | Posted: 21 June 2022 doi:10.20944/preprints202206.0287.v1

or formamide-catalyzed [60] phosphorylation of the nucleosides [61], but these reactions will not be considered here). This stationary state coupling of reactions to diffusion, leading to symmetry breaking (i.e. particular regions of high concentration of the products), was shown to occur for purely thermal reactions with different activator and inhibitor diffusion rates by Turing [62] and studied more generally as *dissipative structures* under the framework of Classical Irreversible Thermodynamic (CIT) theory by Glansdorff and Prigogine [63].

3.2. The Kinetic Equations

Nomenclature, chemical formula, and abbreviations used throughout the text for the concentrations of the participating chemical species involved in the photochemical reactions leading to the purines shown in figure 1 are given in table 1. Their photon extinction coefficients, polar surface area, and dipole moments (related to permeability of the vesicle wall), are also given.

Table 1. Nomenclature, chemical formula, abbreviation (used in the text and in kinetic equations), label in figure 1, wavelength of maximum absorption λ_{max} (see figure 2 of reference [26]), molar extinction coefficient at that wavelength ϵ_{max}, electric dipole moment μ, and the topological polar surface area (TPSA), of the molecules involved in the photochemical synthesis of the purines. Values marked with "*" are estimates, obtained by comparing to similar molecules, for cases where no published data have been found.

Name	chemical formula	abbrev. in text	abbrev. in kinetics	Fig. 1	λ_{max} nm	ϵ_{max} M^{-1} cm^{-1}	μ [D]	TPSA [Å^2]
hydrogen cyanide	HCN	HCN	H	1			2.98	23.8
cyanogen	NCCN	NCCN	Cg	10			0.00	47.6
formamide	H_2N-CHO	formamide	F		220	60 [64,65]	4.27 [66]	43.1
formimidic acid	H(OH)C=NH	formimidic acid (trans)	Fa		220	60	1.14 [66]	43.1 *
ammonium formate	NH_4HCO_2	ammonium formate	Af				+/-, 2.0 *	41.1
diaminomaleonitrile	$C_4H_4N_4$	cis-DAMN (DAMN)	C	2	298	14000 [67]	6.80 [68]	99.6
diaminofumaronitrile	$C_4H_4N_4$	trans-DAMN (DAFN)	T	3	313	8500 [67]	1.49 [68]	99.6
2-amino-3-iminoacrylimidoyl cyanide	$C_4H_4N_4$	AIAC	J	4	275	9000 [5,47]	1.49	99.6 *
4-aminoimidazole-5-carbonitrile	$C_4H_4N_4$	AICN	I	7	250	10700 [67]	3.67	78.5
4-aminoimidazole-5-carboxamide	$C_4H_6N_4O$	AICA	L	10	266 [69]	10700 *	3.67 *	97.8
5-(N′-formamidinyl)-1H-imidazole-4-carbonitrileamidine	$C_5H_5N_5$	amidine	Am		250	10700 [70]	6.83 *	80.5 *
adenine	$C_5H_5N_5$	adenine	A	8	260	15040 [71]	6.83 [72]	80.5
hypoxanthine	$C_5H_4N_4O$	hypoxanthine	Hy	9	250	12500 [73]	3.16	70.1
xanthine	$C_5H_4N_4O_2$	xanthine	Xa	12	268 [5]	9,300 [3]	4.46 [7]	86.9 [12]
guanine	$C_5H_5N_5O$	guanine	G	11	252 [71]	14,090 [71]	5.45 [74]	96.2 [74]

From an analysis of the experiments [1–13,34,64,67] and time-dependent density functional calculations [47,75] performed in the literature, the chemical and photochemical reactions listed in Table 2 will occur in the photochemical dissipative structuring of the purines from HCN, H_2O, and NCCN. Below we describe in detail only those reactions pertinent to the production of guanine and xanthine from AICN. Reactions leading to AICN and adenine have been described in detail elsewhere (Michaelian [26]).

Preprints (www.preprints.org) | NOT PEER-REVIEWED | Posted: 21 June 2022 doi:10.20944/preprints202206.0287.v1

Table 2. Reactions involved in the photochemical synthesis of the purines (see figure 1). Temperature T is in Kelvin and all kinetic parameters were obtained at pH 7.0.

#	reaction	reaction constants
1	H $\xrightarrow{k_1}$ F	$k_1 = \exp(-14039.0/T + 24.732)$; s^{-1}; hydrolysis of HCN [5,76,77]
2	γ_{220}+ F $\rightarrow$ Fa	$q_2 = 0.05$ [64,65,78–80]
3	γ_{220}+ Fa $\rightarrow$ H + H_2O	$q_3 = 0.03$ [79–81]
4	F $\xrightarrow{k_4}$ Af	$k_4 = \exp(-13587.0/T + 23.735)$; s^{-1}; hydrolysis of formamide [77,80]
5	4H $\xrightarrow{k_5}$ C	$k_5 = 1/(\exp(-\Delta E/RT) + 1) \cdot \exp(-10822.37/T + 19.049)$; M^{-1} s^{-1}; $\Delta E = 0.61$ kcal mol^{-1} [5]
6	4H $\xrightarrow{k_6}$ T	$k_6 = 1/(\exp(+\Delta E/RT) + 1) \cdot \exp(-10822.37/T + 19.049)$; M^{-1} s^{-1}; tetramization[5]
7	4H + T + Cg $\xrightarrow{k_7}$ C + T + Cg	$k_7 = (1.0/(1.0 \cdot 0.01)) \exp(-(10822.37 - 728.45)/T + 19.049)$; M^{-2} s^{-1} [5]
8	4H + T + Cg $\xrightarrow{k_8}$ 2T + Cg	$k_8 = k_7$; M^{-2} s^{-1} [5]
9a	γ_{298} + C $\rightarrow$ T	$q_9 = 0.045$ [67]
9b	γ_{313} + T $\rightarrow$ C	$q_{9r} = 0.020$ [5,47,67]
10	γ_{313} + T $\rightarrow$ J	$q_{10} = 0.006$ [5,47,67]
11	γ_{275} + J $\rightarrow$ I	$q_{11} = 0.583$; T $\rightarrow$ I; $q_{10} \times q_{11} = 0.0034$ [5,47]
12	I $\xrightarrow{k_{12}}$ L	$k_{12} = \exp(-E_a/RT + 12.974)$; s^{-1}; $E_a = 19.93$ kcal mol^{-1}; hydrolysis of AICN [6]
13	I:F + Af $\xrightarrow{k_{13}}$ A + F	$k_{13} = \exp(-E_a/RT + 12.973)$; M^{-1} s^{-1}; $E_a = 6.68$ kcal mol^{-1} [82,83]
14	I:F + Fa $\xrightarrow{k_{14}}$ Am + Fa +H_2O	$k_{14} = \exp(-E_a/RT + 12.613)$; M^{-1} s^{-1}; $E_a = 19.90$ kcal mol^{-1} [84]
15	γ_{250} + Am $\rightarrow$ A	$q_{15} = 0.060$ [70]
16	A $\xrightarrow{k_{16}}$ Hy	$k_{16} = 10^{(-5902/T+8.15)}$; s^{-1}; valid for pH within 5 to 8; hydrolysis of adenine [85,86]
17	L + Cg $\xrightarrow{k_{17}}$ G + H	$k_{17} = \exp(-E_a/RT + 15.52)$; $M^{-1}s^{-1}$; AICA + Cyanogen, $E_a = 18.49$ kcal mol^{-1} [6]
18	G $\xrightarrow{k_{18}}$ Xa	$k_{18} = 10^{(-6330/T+9.40)}$; s^{-1}; valid for pH within 5 to 8; hydrolysis of guanine [85,86]
19	γ_{298} + C $\rightarrow$ C	$q_{19} = 0.955$
20	γ_{313} + T $\rightarrow$ T	$q_{20} = 0.972$
21	γ_{275} + J $\rightarrow$ J	$q_{21} = 0.417$
22	γ_{250} + Am $\rightarrow$ Am	$q_{22} = 0.940$
23	γ_{250} + I $\rightarrow$ I	$q_{23} = 1.000$
24	γ_{266} + L $\rightarrow$ L	$q_{24} = 1.000$
25	γ_{260} + A $\rightarrow$ A	$q_{25} = 1.000$
26	γ_{250} + Hy $\rightarrow$ Hy	$q_{26} = 1.000$
27	γ_{252} + G $\rightarrow$ G	$q_{27} = 1.000$
28	γ_{268} + Xa $\rightarrow$ Xa	$q_{28} = 1.000$

The following is a description of the reactions given in table 2 by reaction number. A detailed description is given only for those reactions relevant to the production of guanine and xanthine. For a detailed description of all other reactions, see Michaelian [26].

1. Hydrogen cyanide HCN (H) hydrolyses to formamide H_2NCOH (F) [5,76,77].
2. A photon-induced tautomerization coverts formamide (F) into formimidic acid (Fa) [64,65,78–80].
3. Formimidic acid (Fa) can, in turn, be photolysed into HCN (H) (or HNC) plus H_2O (dehydration) [79–81].
4. Formamide (F) hydrolyses to ammonium formate (Af) [77,80].
5. HCN (H) thermally polymerizes into $(HCN)_x$. It's most stable tetramer ($x = 4$) is known as cis-diaminomaleonitrile, cis-DAMN (C) [5].
6. HCN (H) can also thermally polymerize into trans-diaminomaleonitrile, trans-DAMN (T) [5].
7. Trans-DAMN (T) and cyanogen (Cg) are good catalysts for the polymerization of 4HCN into cis-DAMN (see Table 6 of Sanchez et al.[5]). The catalytic effect of trans-DAMN on the tetramization of HCN was incorporated into the model by reducing the energy of the activation barrier such as to give the same amplification factor of 12 due to the catalytic effect of the inclusion of 0.01 M trans-DAMN in the HCN solution observed in the experiments of Sanchez et al. [5] at a temperature 20 °C.

The catalytic effect of cyanogen (Cg) is taken to be the same as that of trans-DAMN (T) since Sanchez et al. determined both of these to be strong catalysts [5]. As mentioned above, cyanogen is a precursor needed for guanine obtained from the Lyman-α line (121.6 nm) on middle atmospheric

Preprints (www.preprints.org) | NOT PEER-REVIEWED | Posted: 21 June 2022 doi:10.20944/preprints202206.0287.v1

HCN giving, through photolysis, the CN^- radical with high quantum yield (reaction R177 table 1 of Zahnle [46]), and this can form cyanogen $(CN)_2$ by interacting with a second HCN molecule (reaction R199, table 1 Zahnle).

8. Trans-DAMN also acts as an auto-catalyst for its own thermal production from 4HCN. Cyanogen is also an effective catalyst for this reaction (Table 6 of Sanchez et al. [5]).
9. (a) By absorbing a photon of 298 nm, cis-DAMN (C) transforms (through rotation around a double carbon covalent bond) into trans-DAMN (T). (b) There is also a smaller quantum efficiency for converting trans-DAMN back into cis-DAMN by absorption of a photon at 313 nm [5,47,67].
10. A photon at 313 nm electronically excites trans-DAMN (T) which then transforms into 2-amino-3-iminoacrylimidoyl cyanide, AIAC (J), through proton transfer from one of the amino groups [47].
11. AIAC (J), on absorbing a photon at 275 nm, transforms through photon-induced cyclicization (ring closure) into an azetene intermediate (5 of figure 1) in an electronic excited state, which then transforms to the N-heterocyclic carbene (6 of figure 1) and finally this tautomerizes to give the imidazole, 4-aminoimidazole-5-carbonitrle, AICN (I) (7 of figure 1) [47].
12. The imidazole AICN (I), created in the previous photochemical reaction #11, is converted through hydrolysis to 4-aminoimidazole-5-carboxamide, AICA (L) [6].
13. Interaction of the imidazole AICN (I) with ammonium formate (Af), together with the catalytic effect of formamide (F), leads to adenine (A) [82,83].
14. Adenine (A) can also be obtained through the attachment of HCN (H) to AICN (I) to form amidine (Am), which is a formamide (F) catalyzed thermal reaction involving formimidic acid (Fa) [84].
15. A subsequent tautomerization of amidine (Am) is required (calculated to have a high barrier of about 50 kcal mol^{-1}) which, once overcome by absorbing a photon at 250 nm, allows the system to proceed through a subsequent barrier-less cyclicization to form adenine (A) [70].
16. Hydrolysis of adenine (A) gives hypoxathine (Hy), determined by Zheng and Meng to have a transition state barrier of 23.4 kcal mol^{-1} [75].
17. The combination of AIAC (L) with cyanogen (Cg) (a precursor produced in the middle atmosphere from HCN - see reaction # 7) through a thermal reaction leads to guanine (G) and HCN (H) [6].
18. Hydrolysis of guanine (G) leads to xanthine (Xa) [85,86].
19. to 28. These photochemical reactions represent the absorption (within in a 20 nm region centered on the wavelength of peak absorption) and dissipation through internal conversion at a conical intersection to the ground state on a sub-picosecond time scale. All molecules listed in this set of photo-reactions are photo-stable because of this peaked conical intersection connecting the electronic excited state to the ground state. These reactions, with large quantum efficiencies, represent the bulk of the flow of energy from the incident UVC spectrum to the emitted outgoing ocean surface spectrum in the infrared, and therefore contribute most to photon dissipation, or entropy production.

To simplify the kinetic equations for the photochemical reactions listed in table 2, we assume that the molecules only absorb within a region ± 10 nm of their maximum absorption wavelength λ_{max} and that this absorption is at their maximum molar extinction coefficient ϵ_{max} (Table 1), and finally that these wavelength regions do not overlap for calculating the shadowing effect of molecular concentrations at positions above in the vesicle.

We assume that the vesicle is at the ocean surface and the depth coordinate is divided into $i = 20$ bins of width $\Delta x = 5$ μm and the time step for the recursion calculation for the concentrations is 10 ms. The recursion relation for the factor of light intensity $L_\lambda(i, C)$ for a concentration C of the molecule, at a depth $x(i) = i \cdot \Delta x$ below the ocean surface will be,

$$L_\lambda(i, C(i)) = L_\lambda(i-1, C(i-1)) e^{-\Delta x \cdot \alpha_\lambda} \cdot 10^{-\Delta x \cdot \epsilon_\lambda C(i)} \quad (1)$$

where α_λ is the absorption coefficient of water at wavelength λ and ϵ_λ is the molar extinction coefficient of the particular absorbing substance which has concentration $C(i)$ at $x(i)$.

Preprints (www.preprints.org) | NOT PEER-REVIEWED | Posted: 21 June 2022 doi:10.20944/preprints202206.0287.v1

The kinetic equations giving the increments in concentration after each time step $\Delta t \equiv dt$, for use in a discrete recursion relation, at a depth x below the ocean surface are determined from the reactions listed in table 2 to be the following;

$$\begin{aligned}\frac{dH}{dt} &= D_H\frac{\partial^2 H}{\partial x^2} - k_1 H + d\cdot q_3 I_{220} L_{220}(Fa)\frac{(1-10^{-\Delta x \epsilon_{220}Fa})}{\Delta x} - k_5 H^2 - k_6 H^2 - k_7 H^2 T - k_8 H^2 T + k_{17} LCg \\ &= D_H\frac{\partial^2 H}{\partial x^2} + d\cdot q_3 I_{220} L_{220}(Fa)\frac{(1-10^{-\Delta x \epsilon_{220}Fa})}{\Delta x} - Hk_1 - H^2(k_5+k_6+T(k_7+k_8)) + k_{17} LCg\end{aligned} \tag{2}$$

$$\frac{dCg}{dt} = D_{Cg}\frac{\partial^2 Cg}{\partial x^2} - k_{17} LCg \tag{3}$$

$$\frac{dF}{dt} = D_F\frac{\partial^2 F}{\partial x^2} + k_1 H - d\cdot q_2 I_{220} L_{220}(F)\frac{(1-10^{-\Delta x \epsilon_{220}F})}{\Delta x} - k_4 F - k_{14} IFa \tag{4}$$

$$\frac{dFa}{dt} = D_{Fa}\frac{\partial^2 Fa}{\partial x^2} + d\cdot q_2 I_{220} L_{220}(F)\frac{(1-10^{-\Delta x \epsilon_{220}F})}{\Delta x} - d\cdot q_3 I_{220} L_{220}(Fa)\frac{(1-10^{-\Delta x \epsilon_{220}Fa})}{\Delta x} \tag{5}$$

$$\frac{dAf}{dt} = D_{Af}\frac{\partial^2 Af}{\partial x^2} + k_4 F - k_{13} IAf \tag{6}$$

$$\begin{aligned}\frac{dC}{dt} &= D_C\frac{\partial^2 C}{\partial x^2} + k_5 H^2 + k_7 H^2(T+Cg) - d\cdot q_9 I_{298} L_{298}(C)\frac{(1-10^{-\Delta x \epsilon_{298}C})}{\Delta x} \\ &\quad + d\cdot q_{9r} I_{313} L_{313}(T)\frac{(1-10^{-\Delta x \epsilon_{313}T})}{\Delta x}\end{aligned} \tag{7}$$

$$\begin{aligned}\frac{dT}{dt} &= D_T\frac{\partial^2 T}{\partial x^2} + k_6 H^2 + k_8 H^2(T+Cg) + d\cdot q_9 I_{298} L_{298}(C)\frac{(1-10^{-\Delta x \epsilon_{298}C})}{\Delta x} \\ &\quad - d\cdot q_{10} I_{313} L_{313}(T)\frac{(1-10^{-\Delta x \epsilon_{313}T})}{\Delta x} - d\cdot q_{9r} I_{313} L_{313}(T)\frac{(1-10^{-\Delta x \epsilon_{313}T})}{\Delta x}\end{aligned} \tag{8}$$

$$\frac{dJ}{dt} = D_J\frac{\partial^2 J}{\partial x^2} + d\cdot q_{10} I_{313} L_{313}(T)\frac{(1-10^{-\Delta x \epsilon_{313}T})}{\Delta x} - d\cdot q_{11} I_{275} L_{275}(J)\frac{(1-10^{-\Delta x \epsilon_{275}J})}{\Delta x} \tag{9}$$

$$\frac{dI}{dt} = D_I\frac{\partial^2 I}{\partial x^2} + d\cdot q_{11} I_{275} L_{275}(J)\frac{(1-10^{-\Delta x \epsilon_{275}J})}{\Delta x} - k_{12} I - k_{13} IAf - k_{14} IFa \tag{10}$$

$$\frac{dL}{dt} = D_L\frac{\partial^2 L}{\partial x^2} + k_{12} I - k_{17} LCg \tag{11}$$

$$\frac{dAm}{dt} = D_{Am}\frac{\partial^2 Am}{\partial x^2} + k_{14} IFa - d\cdot q_{15} I_{250} L_{250}(Am)\frac{(1-10^{-\Delta x \epsilon_{250}Am})}{\Delta x} \tag{12}$$

$$\frac{dA}{dt} = D_A\frac{\partial^2 A}{\partial x^2} + d\cdot q_{15} I_{250} L_{250}(Am)\frac{(1-10^{-\Delta x \epsilon_{250}Am})}{\Delta x} + k_{13} IAf - k_{16} A \tag{13}$$

$$\frac{dHy}{dt} = D_{Hy}\frac{\partial^2 Hy}{\partial x^2} + k_{16} A \tag{14}$$

$$\frac{dG}{dt} = D_G\frac{\partial^2 G}{\partial x^2} + k_{17} LCg - k_{18} G \tag{15}$$

$$\frac{dXa}{dt} = D_{Xa}\frac{\partial^2 Xa}{\partial x^2} + k_{18} G \tag{16}$$

where the differentials are calculated discretely (e.g. $dH/dt \equiv \Delta H/\Delta t$) and all concentrations are calculated at discrete time steps of $\Delta t = 10$ ms and the calculated value of the change (e.g. $\Delta H(j)/\Delta t$) for time step j is summed to the previous value (e.g. $H(j-1)$). The day/night factor d is equal to 1 during the day and 0 at night. I_{220}, I_{298}, I_{313}, I_{275} and I_{250} are the intensities of the photon fluxes at 220, 298, 313, 275 and 250 nm respectively (see figure 2 of Michaelian [26]). ϵ_λ are the coefficients of molar extinction for the relevant molecule at the corresponding photon wavelengths λ.

Preprints (www.preprints.org) | NOT PEER-REVIEWED | Posted: 21 June 2022 doi:10.20944/preprints202206.0287.v1

3.3. Vesicle Permeability and Internal Diffusion

The permeability of the fatty acid vesicle wall to molecules will decrease both with increasing size of the molecule and with increasing size of its electric dipole moment, and increase with temperature. It is interesting to note that almost all of the final and intermediate product molecules have large sizes and large dipole moments compared with the precursors, implying a tendency towards entrapment within the vesicle. We assume that the vesicle is completely permeable to H_2O, HCN (H) formimidic acid (Fa) and cyanogen (Cg) but impermeable to all the other intermediate and final products. Note that ammonium formate (produced within the vesicle in reaction #4) would be in its ionic form and therefore also unable to cross the fatty acid membrane (permeability across lipid membranes are reduced by orders of magnitude if the molecules are polar or charged [87]).

The diffusion constant D_Y for the molecule Y within the inner aqueous region of the vesicle will depend on the interior solution viscosity, which is dependent on the concentration of organic material. Studies of inter-cellular diffusion of nucleotides indicate three factors influencing diffusion rates, besides temperature, at high solute densities; the viscosity of the solvent, collision rate dependent on solute concentration, the size of the molecules, and the binding interactions between molecules [88]. The diffusion constant of adenine in pure water has been determined to be $D_A = 7.2 \times 10^{-6}$ cm^2 s^{-1} [89] while the measured diffusion rates in the cytoplasm of a cell can be as low as 1.36×10^{-6} cm^2 s^{-1} [88].

Films of organics and trace metals, with a high density of lipids and other hydrocarbons, produced, for example, by the ultraviolet spectrum of Figure 2 of reference Michaelian [26] on CO_2 saturated water [23], could have been expected on the ocean surface during the Archean. Diffusion constants within this sea surface microlayer would then be significantly smaller than for bulk water. Diffusion rates inside the vesicle will depend on the amount of organic material already existing at the air/water interface captured during the formation of the vesicle (which would have varied considerably from region to region), and on the amount of ongoing organic synthesis within the vesicle.

The Stokes-Einstein relation for the diffusion constant of uncharged spherical molecules is given by,

$$D = \frac{k_B T}{6\pi\eta r} \tag{17}$$

where T is the absolute temperature, η the dynamic viscosity of the solvent, and r the radius of the particle (assumed spherical). For polar solvents such as water, molecules with a charge or dipole moment experience further drag due to the charge-dipole or dipole-dipole interaction [90]. All diffusion constants can, therefore, be approximated relative to that measured for adenine at 300 K through the formula;

$$D_Y = \frac{(2+\mu_A)A_A^{1/2}}{(2+\mu_Y)A_Y^{1/2}} \frac{T}{300} D_A(300), \tag{18}$$

where A_A is the polar surface area of adenine, and μ_A and μ_Y are the dipole momenst of adenine and the molecule Y respectively (Table 1). The factor of 2 in the equation sets the importance of including the dipole moment in the diffusion calculation (Eq. (17)), which is complex but relatively unimportant to the calculated concentrations.

The analysis is performed with the diffusion constant for adenine found in present day cytoplasm (i.e. $D_A(300) \approx 1 \times 10^{-6}$ cm^2 s^{-1}). As an example, using the values given in Table 1 for the molecular dipole moments and their polar areas, and equation (18), in Table 3 we list the results for the diffusion constants of all relevant molecules at 80 °C (353.15 K) with respect to that for adenine at 300 K, $D_A(300)$.

Preprints (www.preprints.org) | NOT PEER-REVIEWED | Posted: 21 June 2022 doi:10.20944/preprints202206.0287.v1

Table 3. Diffusion constants at 80 °C (353.15 K) relative to that of adenine at 300 K (i.e. $d_Y = D_Y(353.15)/D_A(300)$ obtained from equation (18). In this paper, $D_A(300)$ is taken to be 1×10^{-6} cm^2 s^{-1}.

d_H	d_F	d_{Fa},	d_{Af}	d_C	d_T	d_J	d_I	d_L	d_{Am}	d_A	d_{Hy}	d_{Cg}	d_G	d_{Xa}
3.84	2.26	4.52	3.64	1.11	2.81	2.81	1.86	1.66	1.18	1.18	2.16	6.76	1.28	1.55

Cyclical boundary conditions are assumed for diffusion, except for HCN (H), formimidic acid (Fa) and cyanogen (Cg) which, because of their small size and small dipole moment, can permeate the vesicle wall and, therefore, at the wall they are given their fixed value specified in the initial conditions of the environment outside the vesicle (see below). The second order derivatives for calculating the diffusion were obtained using the second order finite difference method with double precision variables.

3.4. Initial Conditions

Miyakawa, Cleaves and Miller [76] estimated the steady state bulk ocean concentration of HCN at the origin of life assuming production, through electric discharge on a neutral atmosphere containing some methane, of radicals which attack N_2, leading to an input rate to the oceans of 100 nmole cm^{-2} y^{-1}, and loss of HCN due to hydrolysis and destruction at submarine vents with a 10 million year cycling time of all ocean water for an ocean of 3 Km average depth. For an ocean of pH 6.5 and temperature of 80 °C, they obtained a value of [HCN]$= 1.0 \times 10^{-10}$ M [76].

Not included in the Miyakawa et al. caculation, however, is, as mentioned above, the fact that HCN can also be produced through the solar Lyman alpha line (121.6 nm) photo-lysing N_2 in the upper atmosphere giving atomic nitrogen which then combines with CH and CH_2 to give HCN, or through 145 nm photolysis of CH_4 leading to a CH^* radical which attacks N_2 to give HCN [42]. Including this UV production would increase the input of HCN concentration to the oceans by a factor of at least 6 [46,91,92]. More importantly, the first $\sim$ 100 μm of the ocean surface is now known to be a unique region (the hydrodynamic boundary layer) where surface tension leads to enriched organics with densities up to 10^4 times that of organic material in the water column slightly below [93]. Trace metal enhancement in this microlayer can be one to three orders of magnitude greater than in the bulk [93,94]. Langmuir circulation, Eddy currents, and the scavenging action of bubbles are what tend to concentrate organic material into this surface film. If disturbed, or mixed, the film rapidly reestablishes its integrity. This high density of organic material trapped through hydrophobic and ionic interactions at the ocean surface leads to significantly lower rates of diffusion within the surface microlayer as compared to the ocean bulk [93]. Little diffusion and turbulence imply little mixing. The ocean microlayer is, therefore, a very stable layer which would not be recycled through ocean vents and thus allowed to accumulate. Finally, although HCN is very soluble in bulk water, molecular dynamic simulations have shown that it concentrates to about an order of magnitude larger at the air-water interface due to lateral HCN dipole-dipole interactions, and that HCN evaporates at lower rates than water [95].

Therefore, rather than assuming the low bulk concentrations of Miyakawa et al., we instead consider a higher initial surface concentrations for HCN (H) and cyanogen (Cg) of 6×10^{-5} and for formamide (F) and formimidic acid (Fa) of 1×10^{-5}, the latter resulting from a photochemical tautomerization of formamide, the hydrolysis product of HCN (reactions #1 and #2 of Table 2). We also allow for perturbation of the system by considering the probable existence of small and sparse patches of much higher concentrations, up to 0.1 M of HCN, cyanogen, and formimidic acid, justified by the above mentioned characteristics of the ocean microlayer and the dipole-dipole interaction between HCN molecules. The initial concentrations of all other reactants inside the vesicle (assumed impermeable to these) are taken to be 1.0×10^{-10} M.

 doi:10.20944/preprints202206.0287.v1

4. Results

4.1. Evolution of the Concentration Profile

In Michaelian [26] we have validated our photochemical reaction-diffusion model by comparing results to experimental data for the time dependence of a number of different intermediate products.

In figures 3 through 5 we present the concentrations as a function of time in Archean days (16 hours) of the relevant molecules in the dissipative photochemical synthesis of adenine and guanine inside the vesicle, obtained by solving simultaneously the differential kinetic equations, (2) through (16), for the initial conditions and diffusion constants listed in the figure captions.

The concentration profiles of the molecules evolve over time because of accumulation of photo-products within the vesicle and through a deliberate external perturbation of the non-linear system at 10.4 days which leads it to a new stationary state in which conversion of the environmental precursor molecules HCN and cyanogen into adenine and guanine occurs at greater rates. This leads to greater dissipative efficacy of the system, i.e. to a concentration profile of the product molecules which dissipates more efficiently the incident UVC spectrum.

Preprints (www.preprints.org) | NOT PEER-REVIEWED | Posted: 21 June 2022 doi:10.20944/preprints202206.0287.v1

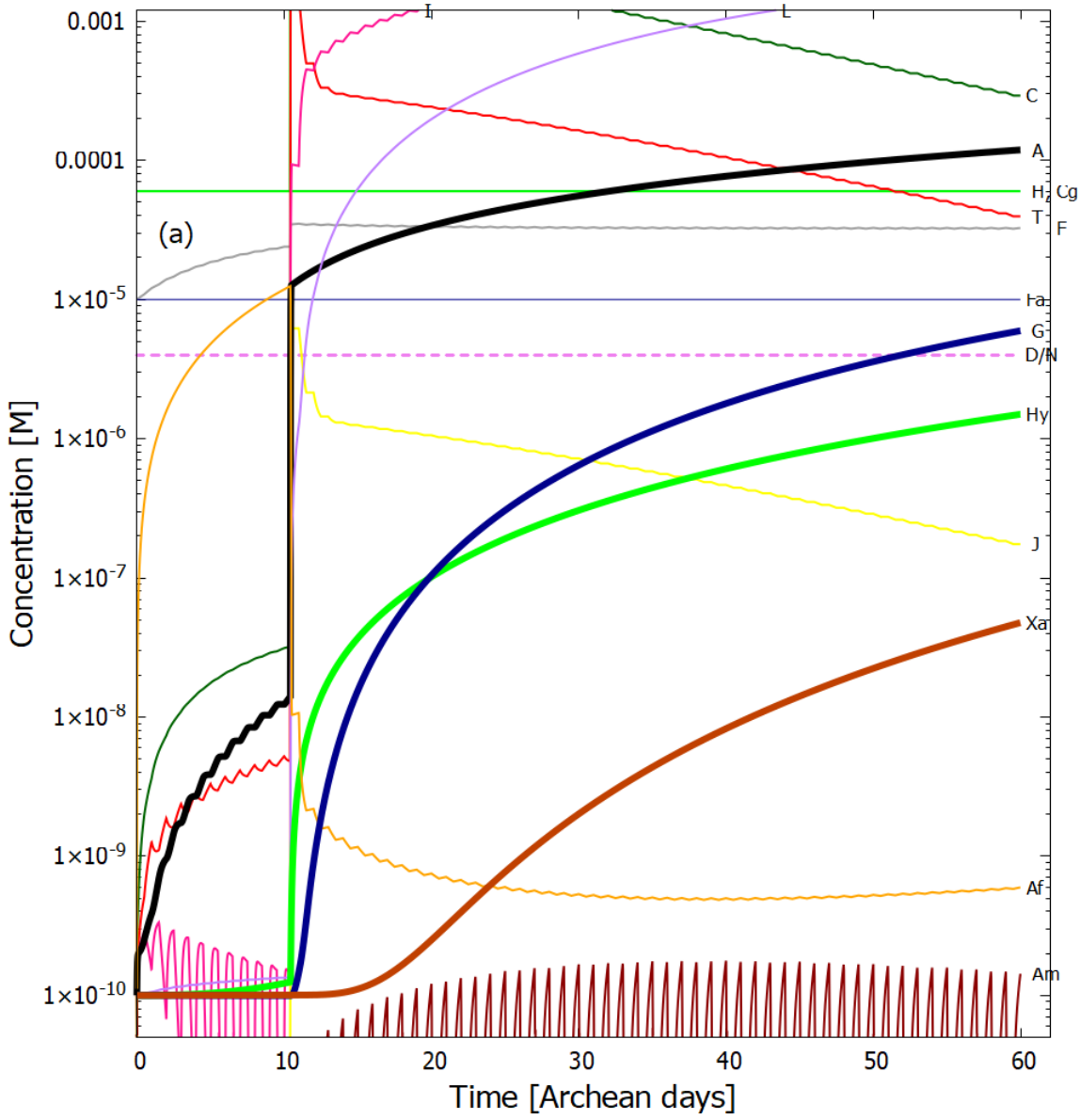

Figure 3. Concentrations as a function of time in Archean days (16 hours) of the precursor and product molecules; H - HCN, F - formamide, Fa - formimidic acid, Cg - cyanogen, Af - ammonium formate , C - cis-DAMN, T - trans-DAMN, A - adenine, I - AICN, J - AIAC, L - AICA, Am - amidine, Hy - hypoxanthine, G - guanine, Xa - xanthine, dissipatively structured on route to the synthesis of adenine (black trace) and guanine (blue trace). The initial conditions are; T=90 °C, initial concentrations $[H]_0$ and $[Cg]_0 = 6.0 \times 10^{-5}$ M, $[F]_0$ and $[Fa]_0 = 1.0 \times 10^{-5}$ M and all other initial concentrations $[Y]_0 = 1.0 \times 10^{-10}$ M. The diffusion constant factor $D_A(300)$ was 1.0×10^{-6} cm^2 s^{-1}. There is one perturbation of the system corresponding to the vesicle floating into a region of HCN (H), cyanogen (Cg), and formimidic acid (Fa) of concentration 0.1 M each for two minutes at 10.4 Archean days. A new stationary state at much higher adenine and guanine concentration is reached after the perturbation. The violet horizontal dashed line labled "D/N" identifies alternate periods of daylight (violet) and night (blank). After 60 Archean days, the concentration of adenine within the vesicle (black trace) has grown by more than six orders of magnitude, from 1.0×10^{-10} to 1.19×10^{-4} M and guanine (blue trace) by 5 orders of magnitude to 3.20×10^{-5} M.

Preprints (www.preprints.org) | NOT PEER-REVIEWED | Posted: 21 June 2022 doi:10.20944/preprints202206.0287.v1

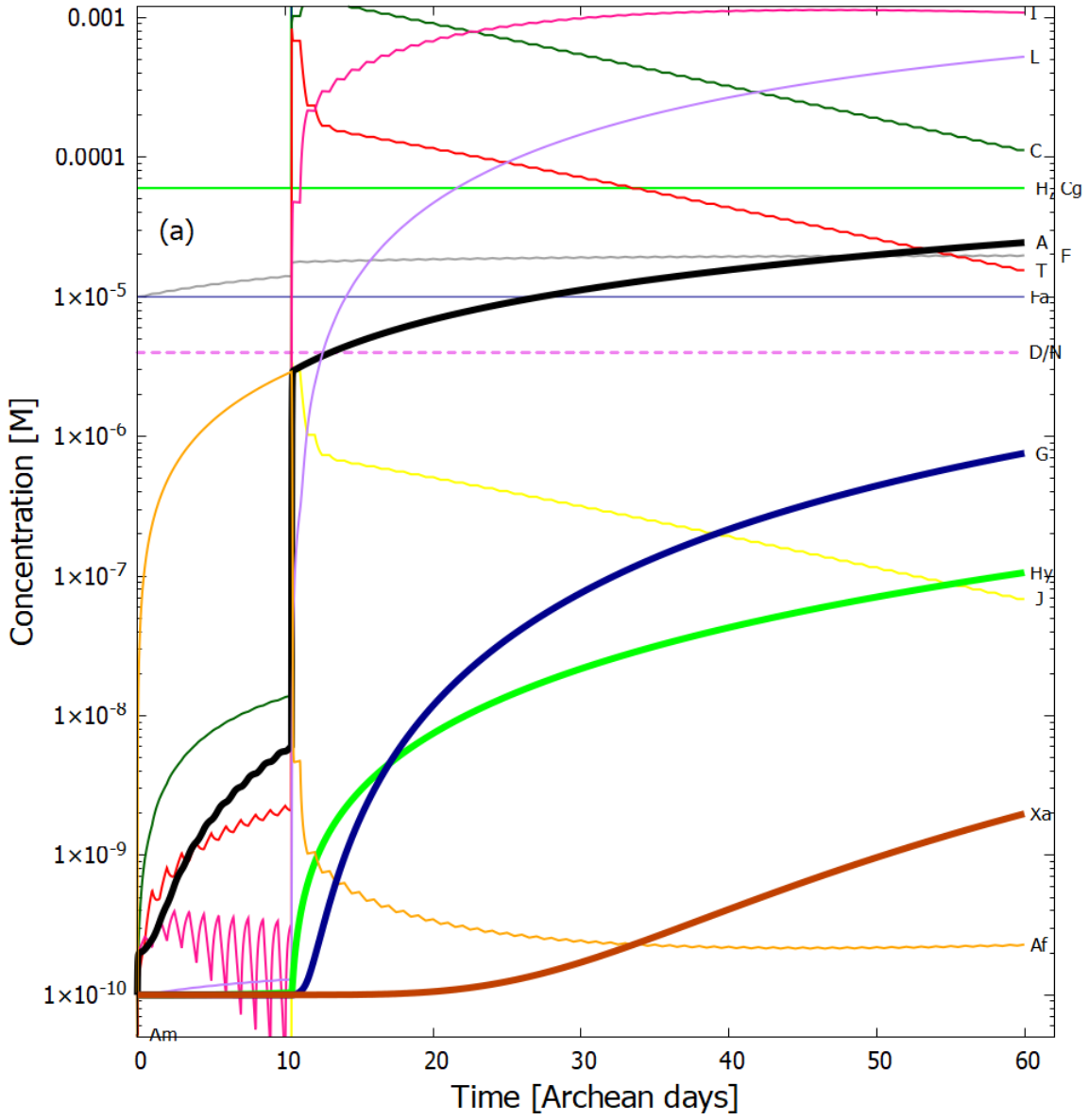

Figure 4. The same as for Fig. 3 except for a temperature of 80 °C. The adenine concentration reaches 2.4×10^{-5} M and a guanine concentration of 7.6×10^{-7} M after 60 Archean days.

Preprints (www.preprints.org) | NOT PEER-REVIEWED | Posted: 21 June 2022 doi:10.20944/preprints202206.0287.v1

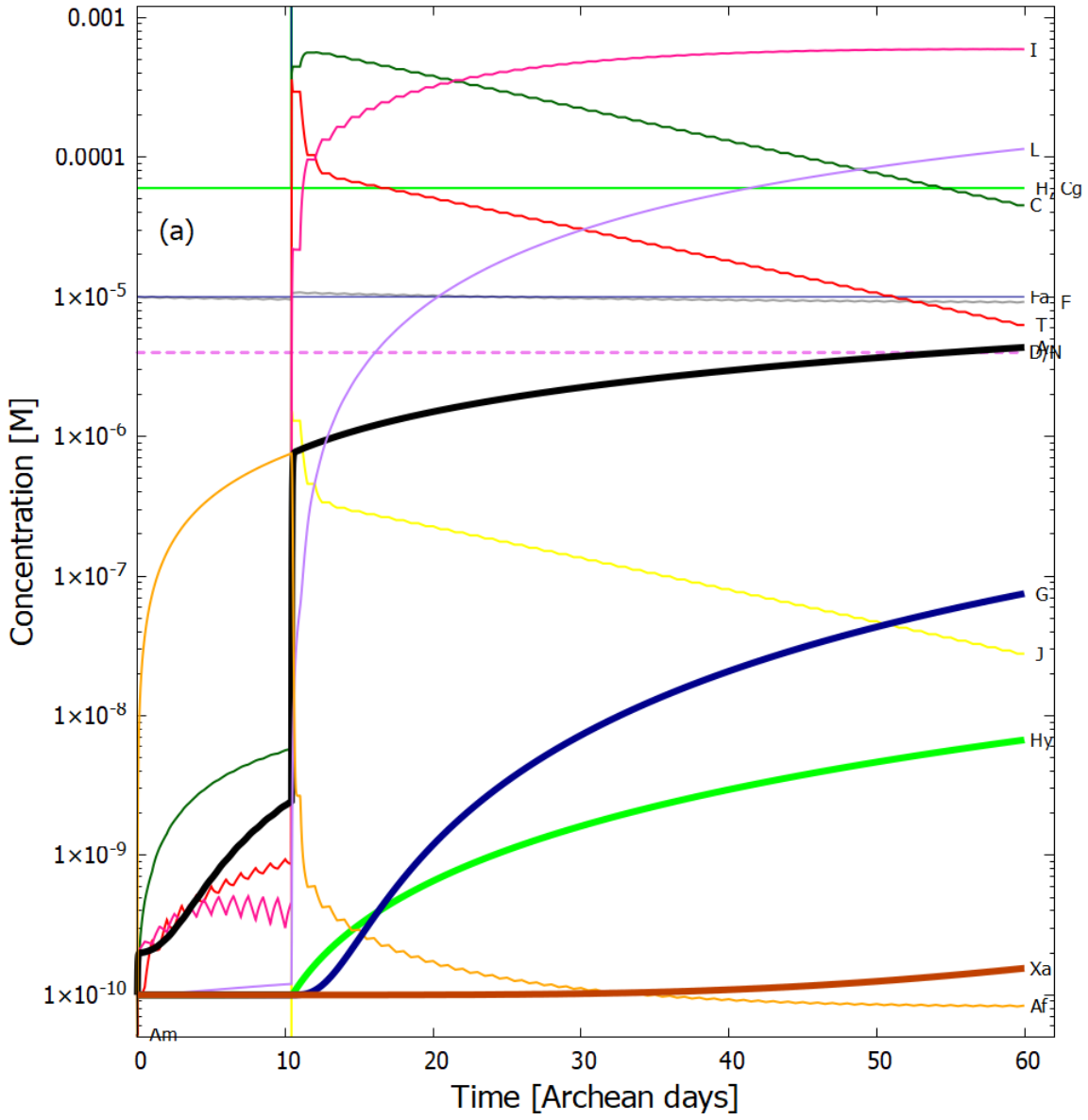

Figure 5. The same as for Fig. 3 except for a temperature of 70 °C. The adenine concentration reaches 4.3×10^{-6} M and a guanine concentration of 7.5×10^{-8} M after 60 Archean days.

Our resulting adenine concentrations are between about 1 and 2 orders of magnitude greater than those of guanine and this is consistent with experimental data of Levy et al. [10] using ammonium cyanide as a precursor under long time eutectic freezing conditions. This greater difficulty of producing guanine abiotically through both processes may explain the fact that the major energy storage molecule of life is adenine triphosphate (ATP) rather than guanine triphosphate (GTP).

Given the fixed concentrations of HCN (H), cyanogen (Cg) and formimidic acid (Fa) in the environment, to which the vesicle is permeable, photochemical reactions occur during daylight hours (denoted as violet colored sections of the horizontal dashed line labeled as D/N). This gives rise to the observable diurnal oscillations in the concentrations of trans-DAMN (T) and AICN (I) since these are direct products of photochemical reactions.

At 10.4 Archean days, the vesicle is perturbed by assuming it passes through a region of high density of HCN (H), cyanogen, and formimidic acid (Fa), each of 0.1 M, for a 2 minute period (vertical lines at 10.4 days). This sudden impulse in HCN, cyanogen, and formimidic acid concentration

Preprints (www.preprints.org) | NOT PEER-REVIEWED | Posted: 21 June 2022 doi:10.20944/preprints202206.0287.v1

gives rise to rapid increases in all concentrations within the vesicle, in particular formamide (F), the hydrolysis product of HCN, which is an important catalyst for reaction #13 which produces adenine (A) from AICN (I) (see Table 2) and this reaction has a low activation barrier energy. Ammonium formate (Af) is used up in this reaction so its concentration decreases rapidly after the perturbation. More importantly, however, immediately after the perturbation there is a greater production of trans-DAMN (T) in the vesicle and since T acts as a catalyst for the polymerization of HCN (H) (reactions #7 and #8), this produces greater metabolism of HCN into DAMN within the vesicle, leading to a stronger diffusion of HCN into the vesicle from the outside environment. In other words, the reason that a short impulse of HCN, cyanogen, and formimidic acid give rise to an important increase in the rate of production of adenine and guanine is that the vesicle's semi-permeable wall, together with the set of equations describing the photochemical and chemical reactions, Eqs. (2-16), form a non-linear (auto- and cross-catalytic) system with multiple solutions at any given time.

The perturbation at 10.4 days causes the system to leave the attraction basin of one solution determined by its initial conditions and evolve towards a different, and more probable, stationary state with a higher rate of production of adenine and guanine (slope of the black and blue traces respectively of figure 4). The new stationary state is more stable than the initial state because its concentration profile is more dissipative, i.e. with more molecules having conical intersections dissipating the absorbed photon energy rapidly into heat, and, therefore, there is less probability of photochemical reactions reverting the concentration profile to the initial state. There is thus a thermodynamic driving force for evolution to the new stationary state after the perturbation due to the system obtaining a greater photon dissipative capacity. For systems where local thermodynamic equilibrium is valid (see Section 3 of Michaelian [26]), this is the same as saying that the entropy production of the system increases (see Figure 7). This is an example of the dissipative structuring a UVC pigment concentration profile, which, we suggest [26], was the physics and chemistry behind a thermodynamic selection relevant to biological evolution at its earliest stages.

It is instructive to compare our overall non-equilibrium results obtained with the model of UVC dissipative structuring of adenine from HCN within a lipid vesicle at 80 °C with the quasi-equilibrium experiments of Ferris et al. [69] using high HCN concentration, alkaline pH, and room temperature. Starting with a concentration of HCN (0.1 M) in water (pH 9.2), and allowing this solution to polymerize in the dark at room temperature for a 7 month period, and then subjecting these polymers to hydrolysis at 110 °C for 24 hours, Ferris et al. obtain an adenine yield of 1 mg L^{-1} , equivalent to a concentration of 7.4×10^{-6} M (the molar mass of adenine being 135.13 g mol^{-1}). Our model gives a similar adenine concentration at about 26 Archean days (Fig. 4), starting from a much lower and more realistic initial concentration of HCN of only 6.0×10^{-5} M (with only one perturbation of 0.1 M for two minutes) and a more probable Archean neutral pH of 7.0 at 80 °C and under a UVC flux integrated from 210 – 280 nm of about 4 W m^{-2} during daylight hours (Figure 4). At 90 °C our adenine concentration within the vesicle surpasses this value after the perturbation at 10.4 days (Fig. 3).

The temperature dependence of the concentrations of the product molecules obtained after 60 Archean days is given in figure 6. Ammonium formate (Af) is produced by the hydrolysis of first HCN (H) to formamide (F) (reacrion #1) and then hydrolysis of formamide to Af (reaction #4). Both of these reactions have high activation energies and this results in Af only being produced in quantities at temperatures greater than 80 °C. Most of the adenine (A) production occurs through reaction #13 which consumes Af and therefore high temperatures are important to the production of adenine for this set of reactions. The hydrolysis of AICN to AICA (step 7 to 10 of figure 1) also has a high activation energy barrier (reaction #12), requiring also high temperatures for the production of guanine (G) and xanthine (Xa).

Preprints (www.preprints.org) | NOT PEER-REVIEWED | Posted: 21 June 2022 doi:10.20944/preprints202206.0287.v1

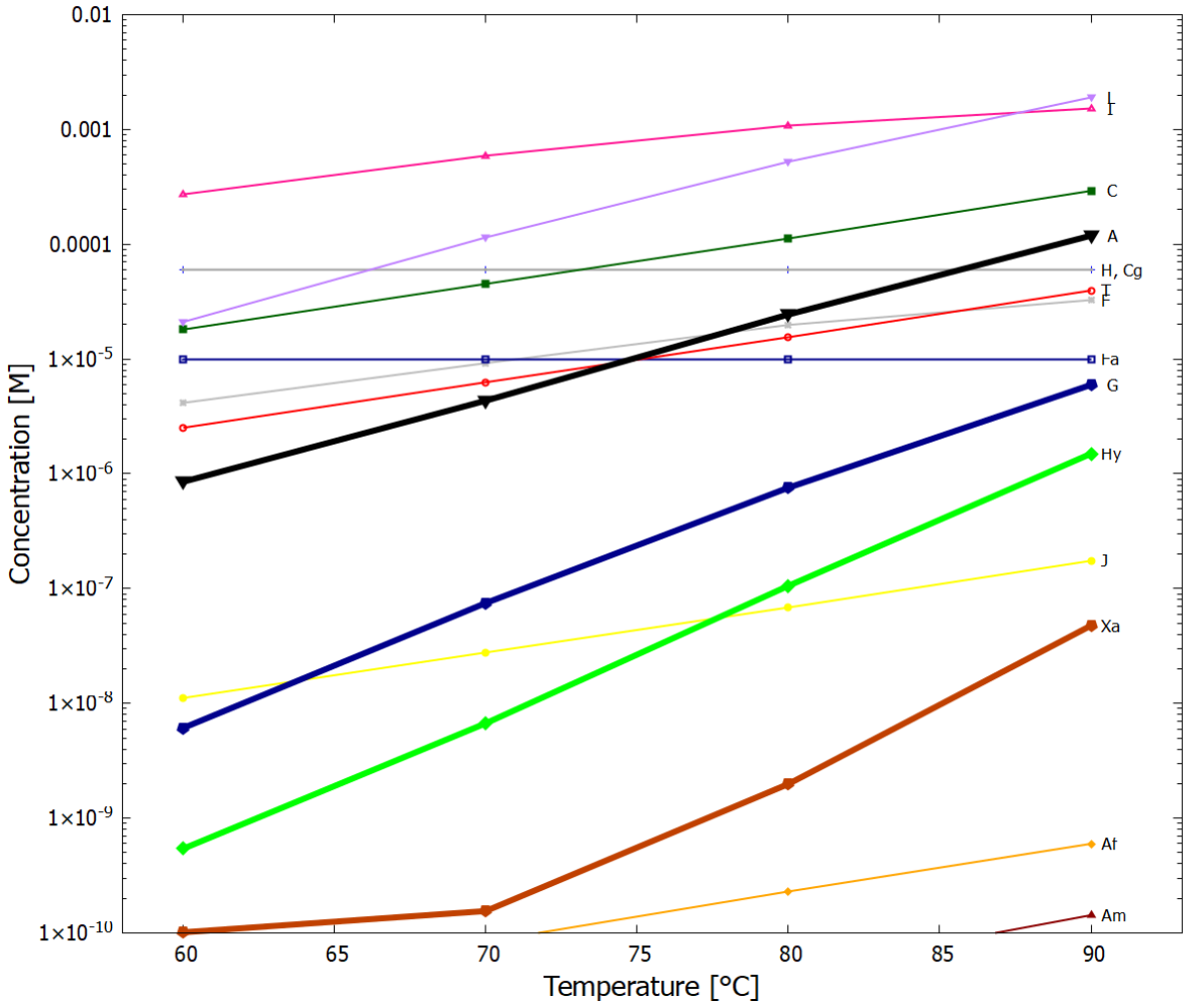

Figure 6. The temperature dependence of the concentrations of the product molecules after 60 Archean days, with the initial conditions, $[H]_0 = 6 \times 10^{-5}$, $[Cg]_0 = 6 \times 10^{-5}$, $[F]_0 = 1 \times 10^{-5}$, $[Fa]_0 = 1 \times 10^{-5}$ M, and all other molecules $[Y]_0 = 1 \times 10^{-10}$ and the diffusion constant $D_A(300) = 1.0 \times 10^{-6}$, with one perturbation of [H], [Cg], [F], and [Fa] to 0.1M for 2 minutes at 10.4 Archean days.

In figure 7 we plot the entropy production as a function of time in Archean days due to solely the photon dissipation associated with the corresponding molecular concentration profile as represented by reactions 19 to 28 of table 2. For a description of the entropy production and its relation to the Glansdorff-Prigogine universal evolutionary criterion, see reference Michaelian [26].

Preprints (www.preprints.org) | NOT PEER-REVIEWED | Posted: 21 June 2022 doi:10.20944/preprints202206.0287.v1

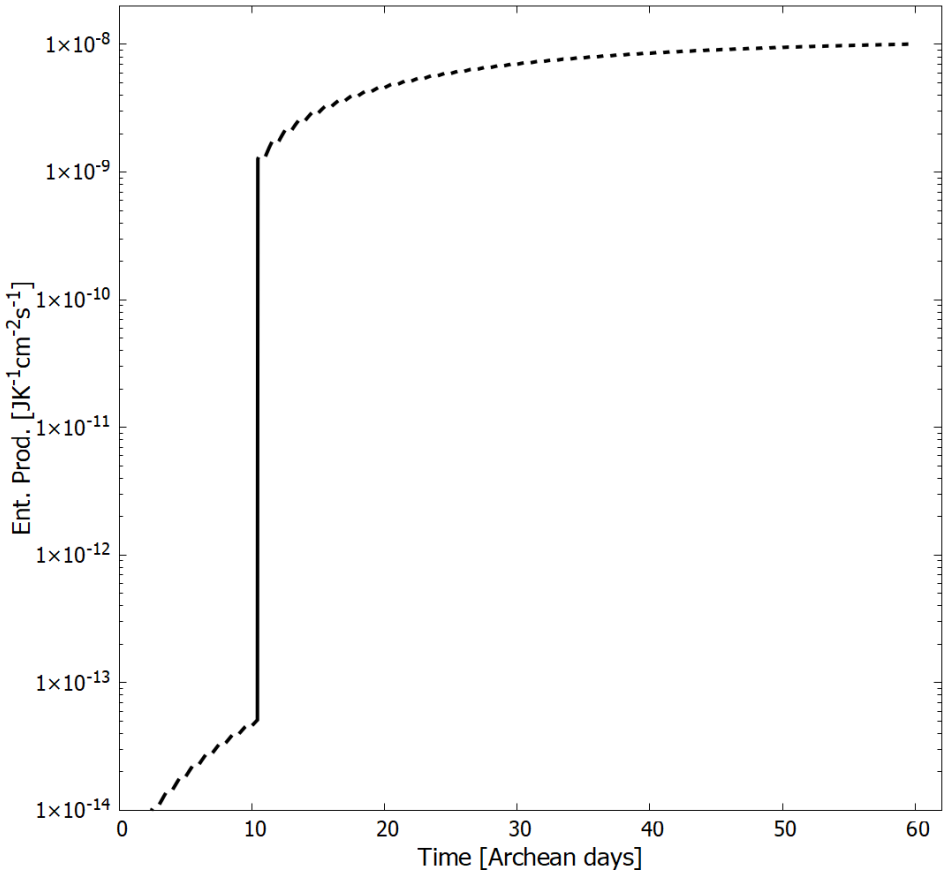

Figure 7. The entropy production as a function of Archean days for our UVC photochemical dissipative structuring process leading to the purines within a vesicle floating at a sea surface at a temperature of 80 °C. Only the entropy production due to photon dissipation by all molecules is included. This entropy production increases monotonically as photochemical reactions convert HCN into the photon dissipative product molecules, including adenine and guanine. During the day, entropy production is due to the dissipation of the UVC spectrum into heat by the corresponding product concentration profile. At night, entropy production goes to zero (although thermal chemical reactions still occur during the night, this entropy production is small and not included in the figure). At 10.4 Archean days, the system is perturbed and the entropy production increases discretely by more than 4 orders of magnitude and continues to increase as the concentration profile changes (see Figure 4).

5. Discussion

High temperatures lead to a faster buildup of product concentration (Fig. 6) and high temperatures would also foment phosphorylation with phosphate salts and formamide, favoring the formation of acyclonucleosides and the phosphorylation and trans-phosphorylation of nucleosides which only occurs efficiently at temperatures above 70 °C [59,60]. These are yet other reasons for favoring a hot origin of life.

As we have detailed in Michaelian [26], besides entrapment of product molecules inside the vesicle, another concentration mechanism for these molecules may arise through the coupling between reaction and diffusion in the non-linear regime which leads to the breaking of spatial symmetry. For low diffusion rates, the homogeneous stationary state is no longer stable with respect to space dependent perturbations and intermediate and final products may become preferentially concentrated and be consumed in the center of the vesicle (see Michaelian [26]).

Inorganic catalysts, which have not been included in our reaction scheme, can increase the rate of purine production. For example Cu^{+2} ions have a large effect in increasing the rate constant for

 doi:10.20944/preprints202206.0287.v1

the conversion of HCN (H) to cis-DAMN (C) [5] (reaction # 5). Cu^{+2} ions also reduce the energy difference (but not the barrier crossing height) between the isomers formimidic and formamidic acid of formamide [96]. Metal ions would have been in high abundance at the ocean surface microlayer [93,97].

The dissipative structuring of the pyrimidines under the same Archean UV wavelength region as for the purines (adenine and guanine), will be considered in a future article.

6. Summary and Conclusions

We have presented a simple kinetic model of UVC photochemical dissipative structuring of the purines. The model is based on published experimental and *ab initio* data for chemical and photochemical reactions. The synthesis of the purines proceeds from HCN and cyanogen in water solvent within a lipid vesicle permeable to H_2O, HCN, cyanogen, and formimidic acid, but impermeable to the reaction products, floating on the hot ocean surface under UVC light. The surface physical conditions being consistent with geochemical fossil evidence from the early Archean.

Important concentrations of all purines buildup within the vesicle within only about 60 Archean days. There is no need to begin with large initial concentrations of HCN by invoking freezing temperature eutectic concentration and there is no need for highly alkaline conditions in order to favor HCN polymerization over hydrolysis.

Perturbations, caused by the vesicle floating into patches of higher concentration of HCN and formimidic acid existing at isolated regions of the ocean surface microlayer, can provoke the non-linear autocatalytic system into new states of higher product productivity with a greater "metabolism" of precursor molecules (HCN and cyanogen) from the environment leading to concentration profiles of greater photon dissipative efficacy.

Evolution is towards concentration profiles of product molecules with an absorption maximum closer to the peak intensity of the incident UVC spectrum and with peaked conical intersections to internal conversion, both increasing the overall efficacy of dissipation of the incident UVC solar spectrum.

For low diffusion rates, there can be significant coupling of reactions with diffusion, leading to non-homogeneous distributions of some of the intermediate products, with greater concentration of these at the center of the vesicle (see Michaelian [26]). Such spatial symmetry breaking could facilitate further structuring such as polymerization of the nucleobases into nucleic acid.

Dissipative structuring, dissipative proliferation, and dissipative selection are the necessary and sufficient ingredients for an explanation in physical-chemical terms of the synthesis, proliferation, and evolution of organic molecules on planets, comets, asteroids, and interstellar space [18], and, in particular, as we have shown here, for explaining the origin and evolution of the fundamental molecules of life on Earth.

Funding: This research was funded by DGAPA-UNAM grant number IN104920.

Acknowledgments: The authors are grateful to a number of anonymous referees for their revision of, and suggestions on, the manuscript.

Conflicts of Interest: The authors declare no conflict of interest.

Abbreviations

The following abbreviations are used in this manuscript:

AIAC	2-amino-3-iminoacrylimidoyl cyanide
AICA	4-aminoimidazole-5-carboxamide
AICN	4-aminoimidazole-5-carbonitrile
CIT	Classical Irreversible Thermodynamics
DAMN	diaminomaleonitrile
DAFN	diaminofumaronitrile
PAHs	Polyaromatic Hydrocarbons
UVA	light in the region 360-400 nm
UVB	light in the region 285-360 nm (only the region 310-360 nm is relevant here)
UVC	light in the region 100-285 nm (only the region 210-285 nm is relevant here)
UVTAR	Ultraviolet and Temperature Assisted Replication

References

1. Miller, S.L.; Urey, H.C. Origin of Organic Compounds on the Primitive Earth and in Meteorites. *Science* **1959**, *130*, 245.
2. Oró, J. Synthesis of adenine from ammonium cyanide. *Biochem. Biophys. Res. Commun.* **1960**, *2*, 407–412.
3. Oró, J.; Kimball, A. Synthesis of purines under possible primitive earth conditions: I. Adenine from hydrogen cyanide. *Archives of Biochemistry and Biophysics* **1961**, *94*, 217 – 227. doi:10.1016/0003-9861(61)90033-9.
4. Oró, J.; Kimball, A. Synthesis of purines under possible primitive earth conditions: II. Purine intermediates from hydrogen cyanide. *Archives of Biochemistry and Biophysics* **1962**, *96*, 293 – 313. doi:10.1016/0003-9861(62)90412-5.
5. Sanchez, R.A.; Ferris, J.P.; Orgel, L.E. Studies in Prebiodc Synthesis II: Synthesis of Purine Precursors and Amino Acids from Aqueous Hydrogen Cyanide. *J. Mol. Biol.* **1967**, *80*, 223–253.
6. Sanchez, R.A.; Ferris, J.P.; Orgel, L.E. Studies in Prebiodc Synthesis IV: Conversion of 4-Aminoimidazole-5-carbonitrile Derivatives to Purines. *J. Mol. Biol.* **1968**, *38*, 121–128.
7. Schwartz, A.; Goverde, M. Acceleration of HCN oligomerization by formaldehyde and related compounds: Implications for prebiotic syntheses. *J Mol Evol* **1982**, *18*, 351–353.
8. Voet, A.; Schwartz, A. Prebiotic adenine synthesis from HCN—Evidence for a newly discovered major pathway. *Bioorganic Chemistry* **1983**, *12*, 8–17. doi:https://doi.org/10.1016/0045-2068(83)90003-2.
9. Levy, M.; Miller, S.L. The Prebiotic Synthesis of Modified Purines and Their Potential Role in the RNA World. *J Mol Evol* **1999**, *48*, 631–637.
10. Levy, M.; Miller, S.L.; Oró, J.J. Production of Guanine from NH4CN Polymerizations. *J Mol Evol* **1999**, *49*, 165–168.
11. Saladino, R.; Crestini, C.; Costanzo, G.; Negri, R.; Di Mauro, E. A possible prebiotic synthesis of purine, adenine, cytosine, and 4(3H)-pyrimidinone from formamide: implications for the origin of life. *Bioorg Med Chem.* **2001**, *9*, 1249–1253. doi:10.1016/s0968-0896(00)00340-0.
12. Hill, A.; Orgel, L. Synthesis of Adenine from HCN Tetramer and Ammonium Formate. *Orig Life Evol Biosph* **2002**, *32*, 99–102.
13. Borquez, E.; Cleaves, H.; Lazcano, A.; Miller, S. An Investigation of Prebiotic Purine Synthesis from the Hydrolysis of HCN Polymers. *Orig Life Evol Biosph* **2005**, *35*, 79–90.
14. Michaelian, K. Thermodynamic origin of life. *ArXiv* **2009**, [arXiv:physics.gen-ph/0907.0042]. doi:10.5194/esd-2-37-2011.
15. Michaelian, K. Thermodynamic dissipation theory for the origin of life. *Earth Syst. Dynam.* **2011**, *224*, 37–51, [https://esd.copernicus.org/articles/2/37/2011/esd-2-37-2011.html].
16. Michaelian, K., The Biosphere; INTECH, 2012; chapter The biosphere: A thermodynamic imperative.
17. Michaelian, K. A non-linear irreversible thermodynamic perspective on organic pigment proliferation and biological evolution. *Journal of Physics* **2013**, *Conference Series 475*, 012010, [https://iopscience.iop.org/article/10.1088/1742-6596/475/1/012010/meta].

18. Michaelian, K.; Simeonov, A. Fundamental molecules of life are pigments which arose and co-evolved as a response to the thermodynamic imperative of dissipating the prevailing solar spectrum. *Biogeosciences* **2015**, *12*, 4913–4937, [https://bg.copernicus.org/articles/12/4913/2015/].
19. Michaelian, K. *Thermodynamic Dissipation Theory of the Origina and Evolution of Life: Salient characteristics of RNA and DNA and other fundamental molecules suggest an origin of life driven by UV-C light*; Self-published. Printed by CreateSpace. Mexico City. ISBN:9781541317482., 2016.
20. Michaelian, K.; Simeonov, A. Thermodynamic explanation of the cosmic ubiquity of organic pigments. *Astrobiol. Outreach* **2017**, *5*, 156, [https://www.longdom.org/open-access/thermodynamic-explanation-for-the-cosmic-ubiquity-of-organicpigments-2332-2519
21. Michaelian, K. Microscopic Dissipative Structuring and Proliferation at the Origin of Life. *Heliyon* **2017**, *3*, e00424, [https://www.ncbi.nlm.nih.gov/pmc/articles/PMC5647473/]. doi:10.1016/j.heliyon.2017.e00424.
22. Michaelian, K. Homochirality through Photon-Induced Denaturing of RNA/DNA at the Origin of Life. *Life* **2018**, *8*, [http://www.mdpi.com/2075-1729/8/2/21]. doi:10.3390/life8020021.
23. Michaelian, K.; Rodriguez, O. Prebiotic fatty acid vesicles through photochemical dissipative structuring. *Revista Cubana de Química* **2019**, *31*, 354–370.
24. Michaelian, K.; Santillan, N. UVC photon-induced denaturing of DNA: A possible dissipative route to Archean enzyme-less replication. *Heliyon* **2019**, *5*, e01902, [https://www.heliyon.com/article/e01902].
25. Mejía Morales, J.; Michaelian, K. Photon Dissipation as the Origin of Information Encoding in RNA and DNA. *Entropy* **2020**, *22*, [https://www.mdpi.com/1099-4300/22/9/940]. doi:10.3390/e22090940.
26. Michaelian, K. The Dissipative Photochemical Origin of Life: UVC Abiogenesis of Adenine. *Entropy* **2021**, *23*, [https://www.mdpi.com/1099-4300/23/2/217]. doi:10.3390/e23020217.
27. Michaelian, K.; Mateo, R.E.C. A Photon Force and Flow for Dissipative Structuring: Application to Pigments, Plants and Ecosystems. *Entropy* **2022**, *24*, 76. doi:10.3390/e24010076.
28. Michaelian, K. Non-Equilibrium Thermodynamic Foundations of the Origin of Life. *Foundations* **2022**, *2*, 308–337. doi:10.3390/foundations2010022.
29. Berkner, L.; Marshall, L., Origin and Evolution of the Oceans and Atmosphere; J. Wiley and Sons, 1964; pp. 102–126.
30. Sagan, C. Ultraviolet Selection Pressure on the Earliest Organisms. *J. Theor. Biol.* **1973**, *39*, 195–200.
31. Cnossen, I.; Sanz-Forcada, J.; Favata, F.and Witasse, O.; Zegers, T.; Arnold, N.F. The habitat of early life: Solar X-ray and UV radiation at Earth's surface 4–3.5 billion years ago. *J. Geophys. Res.* **2007**, *112*, E02008. doi:10.1029/2006JE002784.
32. Meixnerová, J.; Blum, J.D.; Johnson, M.W.; Stüeken, E.E.; Kipp, M.A.; Anbar, A.D.; Buick, R. Mercury abundance and isotopic composition indicate subaerial volcanism prior to the end-Archean “whiff” of oxygen. *Proceedings of the National Academy of Sciences* **2021**, *118*, e2107511118, [https://www.pnas.org/doi/pdf/10.1073/pnas.2107511118]. doi:10.1073/pnas.2107511118.
33. Schuurman, M.S.; Stolow, A. Dynamics at Conical Intersections. *Annu. Rev. Phys. Chem.* **2018**, *69*, 427–450.
34. Ferris, J.P.; Orgel, L.E. An Unusual Photochemical Rearrangement in the Synthesis of Adenine from Hydrogen Cyanide. *J. Am. Chem. Soc.* **1966**, *88*, 1074–1074.
35. Sagan, C.; Khare, B.N. Long-Wavelength Ultraviolet Photoproduction of Amino Acids on the Primitive Earth. *Science* **1971**, *173*, 417–420, [https://science.sciencemag.org/content/173/3995/417.full.pdf]. doi:10.1126/science.173.3995.417.
36. Ruiz-Bermejo, M.; Zorzano, M.P.; Osuna-Esteban, S. Simple Organics and Biomonomers Identified in HCN Polymers: An Overview. *Life* **2013**, *3*, 421–448. doi:10.3390/life3030421.
37. Pflüger, E. Beitragë zur Lehre von der Respiration. I. Ueber die physiologische Verbrennung in den lebendigen organismen. *Arch. Ges. Physiol.* **1875**, *10*, 641–644.
38. Ritson, D.; Sutherland, J. Prebiotic synthesis of simple sugars by photoredox systems chemistry. *Nature Chem.* **2012**, *4*, 895–899.
39. Das, T.; Ghule, S.; Vanka, K. Insights Into the Origin of Life: Did It Begin from HCN and H2O? *ACS Central Science* **2019**, *5*, 1532–1540, [https://doi.org/10.1021/acscentsci.9b00520]. doi:10.1021/acscentsci.9b00520.
40. Matthews, C. Dark matter in the solar system: Hydrogen cyanide polymers. *Origins Life Evol Biosphere* **1991**, *21*, 421–434.

41. Matthews, C.; Minard, R. Hydrogen cyanide polymers, comets and the origin of life. *Faraday Discuss.* **2006**, *133*, 393–401. doi:10.1039/b516791d.
42. Trainer, M.G.; Jimenez, J.L.; Yung, Y.L.; Toon, O.B.; Tolbert, M.A. Nitrogen Incorporation in CH_4-N_2 Photochemical Aerosol Produced by Far UV Irradiation. *NASA archives* **2012**, [https://ntrs.nasa.gov/archive/nasa/casi.ntrs.nasa.gov/20120009529.pdf].
43. Pearce, B.K.D.; Molaverdikhani, K.; Pudritz, R.E.; Henning, T.; Hébrard, E. HCN Production in Titan's Atmosphere: Coupling Quantum Chemistry and Disequilibrium Atmospheric Modeling. *The Astrophysical Journal* **2020**, *901*, 110. doi:10.3847/1538-4357/abae5c.
44. Airey, P.L.; Dainton, F.S. The photochemistry of aqueous solutions of Fe(II) II. Processes in acidified solutions of potassium ferrocyanide at 25°C. *Proceedings of the Royal Society of London. Series A. Mathematical and Physical Sciences* **1966**, *291*, 478–486, [https://royalsocietypublishing.org/doi/pdf/10.1098/rspa.1966.0109]. doi:10.1098/rspa.1966.0109.
45. Fox, S.W.; Harada, K. Synthesis of Uracil under Conditions of a Thermal Model of Prebiological Chemistry. *Science* **1961**, *133*, 1923–1924, [https://science.sciencemag.org/content/133/3468/1923.full.pdf]. doi:10.1126/science.133.3468.1923.
46. Zahnle, K.J. Photochemistry of methane and the formation of hydrocyanic acid (HCN) in the Earth's early atmosphere. *Journal of Geophysical Research: Atmospheres* **1986**, *91*, 2819–2834, [https://agupubs.onlinelibrary.wiley.com/doi/pdf/10.1029/JD091iD02p02819]. doi:10.1029/JD091iD02p02819.
47. Boulanger, E.; Anoop, A.; Nachtigallova, D.; Thiel, W.; Barbatti, M. Photochemical Steps in the Prebiotic Synthesis of Purine Precursors from HCN. *Angew. Chem. Int.* **2013**, *52*, 8000–8003.
48. Miller, S.L.; Lazcano, A. The Origin of Life – Did It Occur at High Temperatures? *Mol. Evol.* **1995**, *41*, 689–692.
49. Bada, J.L.; Lazcano, A. Some Like It Hot, But Not the First Biomolecules. *Science* **2002**, *296*, 1982–1983.
50. Miyakawa, S.; Cleaves, H.J.; Miller, S.L. The cold origin of life: B. Implications based on pyrimidines and purines produced from frozen ammonium cyanide solutions. *Origins of Life and Evolution of the Biosphere* **2002**, *32*, 209–218.
51. Oró, J. Chemical synthesis of lipids and the origin of life. *J Biol Phys* **1995**, *20*, 135–147. doi:https://doi.org/10.1007/BF00700430.
52. Walde, P.; Wick, R.; Fresta, M.; Mangone, A.; Luisi, P.L. Autopoietic Self-Reproduction of Fatty Acid Vesicles. *Journal of the American Chemical Society* **1994**, *116*, 11649–11654, [https://doi.org/10.1021/ja00105a004]. doi:10.1021/ja00105a004.
53. Karhu, J.; Epstein, S. The Implication of the Oxygen isotope Records in Coexisting Cherts and Phosphates. *Geochim. Cosmochim. Acta* **1986**, *50*, 1745–1756.
54. Knauth, L.P., Lecture Notes in Earth Sciences #43; Springer-Verlag, Berlin, 1992; chapter Isotopic Signatures and Sedimentary Records, pp. 123–152.
55. Knauth, L.P.; Lowe, D.R. High Archean climatic temperature inferred from oxygen isotope geochemistry of cherts in the 3.5 Ga Swaziland group, South Africa. *Geol. Soc. Am. Bull.* **2003**, *115*, 566–580.
56. Fan, Y.; Fang, Y.; Ma, L. The self-crosslinked ufasome of conjugated linoleic acid: Investigation of morphology, bilayer membrane and stability. *Colloids and Surfaces B: Biointerfaces* **2014**, *123*, 8 – 14. doi:https://doi.org/10.1016/j.colsurfb.2014.08.028.
57. Han, J.; Calvin, M. Occurrence of fatty acids and aliphatic hydrocarbons in a 3.4 billion-year-old sediment. *Nature* **1969**, *224*, 576–577.
58. Van Hoeven, W.; Maxwell, J.; Calvin, M. Fatty acids and hydrocarbons as evidence of life processes in ancient sediments and crude oils. *Geochimica et Cosmochimica Acta* **1969**, *33*, 877–881.
59. Schoffstall, A.M. Prebiotic phosphorylation of nucleosides in formamide. *Origins Life Evol Biosphere* **1976**, *7*, 399–412.
60. Costanzo, G.; Saladino, R.; Crestini, C.; Ciciriello, F.; Di Mauro, E. Nucleoside phosphorylation by phosphate minerals. *J Biol Chem.* **2007**, *282*, 16729–16735. doi:doi:10.1074/jbc.M611346200.
61. Pasek, M.A.; Harnmeijer, J.P.; Buick, R.; Gull, M.; Atlas, Z. Evidence for reactive reduced phosphorus species in the early Archean ocean. *Proceedings of the National Academy of Sciences* **2013**, *110*, 10089–10094, [https://www.pnas.org/doi/pdf/10.1073/pnas.1303904110]. doi:10.1073/pnas.1303904110.

62. Turing, A.M. The Chemical Basis of Morphogenesis. *Philosophical Transactions of the Royal Society of London Series B* **1952**, *237*, 37–72. doi:10.1098/rstb.1952.0012.
63. Glansdorff, P.; Prigogine, I. *Thermodynamic Theory of Structure, Stability and Fluctuations*; Wiley - Interscience., 1971.
64. Petersen, C.; Dahl, N.H.; Jensen, S.K.; Poulsen, J.A.; Thøgersen, J.; Keiding, S.R. Femtosecond Photolysis of Aqueous Formamide. *The Journal of Physical Chemistry A* **2008**, *112*, 3339–3344, [https://doi.org/10.1021/jp7110764]. PMID: 18321081, doi:10.1021/jp7110764.
65. Basch, H.; Robin, M.B.; Kuebler, N.A. Electronic Spectra of Isoelectronic Amides, Acids, and Acyl Fluorides. *The Journal of Chemical Physics* **1968**, *49*, 5007–5018, [https://doi.org/10.1063/1.1669992]. doi:10.1063/1.1669992.
66. Lelj, F.; Adamo, C. Solvent effects on isomerization equilibria: An energetic analysis in the framework of density functional theory. *Theoretica chimica acta* **1995**, *91*, 199–214. doi:10.1007/BF01114987.
67. Koch, T.; Rodehorst, R. Quantitative investigation of the photochemical conversion of diaminomaleonitrile to diaminofumaronitrile and 4-amino-5-cyanoimidazole. *J. Am. Chem. Soc.* **1974**, *96*, 6707–6710.
68. Gupta, V.; Tandon, P. Conformational and vibrational studies of isomeric hydrogen cyanide tetramers by quantum chemical methods. *Spectrochimica Acta Part A: Molecular and Biomolecular Spectroscopy* **2012**, *89*, 55 – 66. doi:https://doi.org/10.1016/j.saa.2011.12.030.
69. Ferris, J.; Joshi, P.; Edelson, E.; Lawless, J. HCN: a plausible source of purines, pyrimidines and amino acids on the primitive Earth. *Journal of molecular evolution* **1978**, *11*, 293–311.
70. Glaser, R.; Hodgen, B.; Farrelly, D.; McKee, E. Adenine synthesis in interstellar space: mechanisms of prebiotic pyrimidine-ring formation of monocyclic HCN-pentamers. *Astrobiology* **2007**, *7*, 455-470. doi:doi:10.1089/ast.2006.0112.
71. Cavaluzzi, M.J.; Borer, P.N. Revised UV extinction coefficients for nucleoside-5′- monophosphates and unpaired DNA and RNA. *Nucleic Acids Research* **2004**, *32*, e13. doi:10.1093/nar/gnh015.
72. Franz, J.; Gianturco, F. Low-energy positron scattering from DNA nucleobases: the effects from permanent dipoles. *Eur. Phys. J. D* **2014**, *68*.
73. Stimson, M.M.; Reuter, M.A. Ultraviolet Absorption Spectra of Nitrogenous Heterocycles. VII. The Effect of Hydroxy Substitutions on the Ultraviolet Absorption of the Series: Hypoxanthine, Xanthine and Uric Acid1. *Journal of the American Chemical Society* **1943**, *65*, 153–155, [https://doi.org/10.1021/ja01242a006]. doi:10.1021/ja01242a006.
74. SC, Y.; SM, Z.; V, S.L.; KH, C. Correlation between polar surface area and bioferroelectricity in DNA and RNA nucleobases. *Eur Phys J E Soft Matter* **2018**, *41*, 86. doi:10.1140/epje/i2018-11696-5.
75. Zheng, H.; Meng, F. Theoretical study of water-assisted hydrolytic deamination mechanism of adenine. *Struct Chem* **2009**, *20*, 943–949.
76. Miyakawa, S.; Cleaves, H.J.; Miller, S.L. The Cold Origin of Life: A. Implications Based On The Hydrolytic Stabilities Of Hydrogen Cyanide And Formamide. *Origins of Life and Evolution of the Biosphere* **2002**, *32*, 195–208.
77. Kua, J.; Thrush, K.L. HCN, Formamidic Acid, and Formamide in Aqueous Solution: A Free-Energy Map. *The Journal of Physical Chemistry B* **2016**, *120*, 8175–8185, [https://doi.org/10.1021/acs.jpcb.6b01690]. PMID: 27016454, doi:10.1021/acs.jpcb.6b01690.
78. Maier, G.; Endres, J. Isomerization of Matrix-Isolated Formamide: IR-Spectroscopic Detection of Formimidic Acid. *European Journal of Organic Chemistry* **2000**, *2000*, 1061–1063, [https://chemistry-europe.onlinelibrary.wiley.com/doi/pdf/10.1002]. doi:10.1002/(SICI)1099-0690(200003)2000:6<1061::AID-EJOC1061>3.0.CO;2-5.
79. Duvernay, F.; Trivella, A.; Borget, F.; Coussan, S.; Aycard, J.P.; Chiavassa, T. Matrix Isolation Fourier Transform Infrared Study of Photodecomposition of Formimidic Acid. *J. Phys. Chem. A* **2005**, *109*, 11155–11162.
80. Barks, H.L.; Buckley, R.; Grieves, G.A.; Di Mauro, E.; Hud, N.V.; Orlando, T.M. Guanine, Adenine, and Hypoxanthine Production in UV-Irradiated Formamide Solutions: Relaxation of the Requirements for Prebiotic Purine Nucleobase Formation. *ChemBioChem* **2010**, *11*, 1240–1243, [https://chemistry-europe.onlinelibrary.wiley.com/doi/pdf/10.1002/cbic.201000074]. doi:10.1002/cbic.201000074.

631 81. Gingell, J.; Mason, N.; Zhao, H.; Walker, I.; Siggel, M. VUV optical-absorption and
632 electron-energy-loss spectroscopy of formamide. *Chemical Physics* **1997**, *220*, 191 – 205.
633 doi:https://doi.org/10.1016/S0301-0104(97)00137-7.
634 82. Yonemitsu, E.; Isshiki, T.; Kijima, Y. Process for preparing adenine, 1974. US Patent 4,059,582.
635 83. Zubay, G.; Mui, T. Prebiotic Synthesis of Nucleotides. *Orig Life Evol Biosph* **2001**, *31*, 87–102.
636 84. Wang, J.; Gu, J.; Nguyen, M.T.; Springsteen, G.; Leszczynski, J. From Formamide to Purine: A Self-Catalyzed
637 Reaction Pathway Provides a Feasible Mechanism for the Entire Process. *The Journal of Physical Chemistry B*
638 **2013**, *117*, 9333–9342, [https://doi.org/10.1021/jp404540x]. PMID: 23902343, doi:10.1021/jp404540x.
639 85. Levy, M.; Miller, S.L. The stability of the RNA bases: Implications for the origin of life. *Proc. Natl. Acad. Sci.*
640 *USA* **1998**, *95*, 7933–7938.
641 86. Wang, S.; Hu, A. Comparative study of spontaneous deamination of adenine and cytosine in
642 unbuffered aqueous solution at room temperature. *Chemical Physics Letters* **2016**, *653*, 207 – 211.
643 doi:https://doi.org/10.1016/j.cplett.2016.05.001.
644 87. Yang, N.J.; Hinner, M.J. Getting Across the Cell Membrane: An Overview for Small Molecules, Peptides,
645 and Proteins. *Methods Mol Biol.* **2015**, *1266*, 29–53. doi:10.1007/978-1-4939-2272-7_3.
646 88. Agarwal, S.; Clancy, C.; Harvey, R. Mechanisms Restricting Diffusion of Intracellular cAMP. *Sci. Rep.* **2008**,
647 *6*, 19577. doi:10.1038/srep19577.
648 89. Bowen, W.J.; Martin, H.L. The diffusion of adenosine triphosphate through aqueous solutions. *Archives of*
649 *Biochemistry and Biophysics* **1964**, *107*, 30 – 36. doi:https://doi.org/10.1016/0003-9861(64)90265-6.
650 90. Samanta, T.; Matyushov, D.V. Dielectric friction, violation of the Stokes-Einstein-Debye relation, and
651 non-Gaussian transport dynamics of dipolar solutes in water. *Phys. Rev. Research* **2021**, *3*, 023025.
652 doi:10.1103/PhysRevResearch.3.023025.
653 91. Chyba, C.F.; Sagan, C. Endogenous production, exogenous delivery and impact-shock synthesis of organic
654 molecules: an inventory for the origins of life. *Nature* **1992**, *355*, 125–132.
655 92. Stribling, R.; Miller, S.L. Energy Yields for Hydrogen Cyanide and Formaldehyde Syntheses: The HCN
656 and Amino Acid Concentrations in the Primitive Ocean. *Origins Life* **1986**, *17*, 261–273.
657 93. Hardy, J.T. The sea-surface Microlayer (1982) Biology, Chemistry and Anthropogenic Enrichment. *Prog.*
658 *Oceanogr.* **1982**, *11*, 307–328.
659 94. Zhang, Z.; Liu, C.; Liu, L.; Yu, L.; Wang, Z. Study on Dissolved Trace Metals in Sea Surface Microlayer in
660 Daya Bay. *Chinese Journal of Oceanology and Limnology* **2004**, *22*, 54 – 63.
661 95. Fábián, B.; Szőri, M.; Jedlovszky, P. Floating Patches of HCN at the Surface of Their Aqueous Solutions
662 – Can They Make "HCN World" Plausible? *The Journal of Physical Chemistry C* **2014**, *118*, 21469–21482,
663 [https://doi.org/10.1021/jp505978p]. doi:10.1021/jp505978p.
664 96. Luna, A.; Morizur, J.P.; Tortajada, J.; Alcamí, M.; Mó, O.; Yáñez, M. Role of Cu+ Association on the
665 Formamide → Formamidic Acid → (Aminohydroxy)carbene Isomerizations in the Gas Phase. *The Journal*
666 *of Physical Chemistry A* **1998**, *102*, 4652–4659, [https://doi.org/10.1021/jp980629c]. doi:10.1021/jp980629c.
667 97. Grammatika, M.; Zimmerman, W.B. Microhydrodynamics of flotation processes in the sea-surface layer.
668 *Dynam. Atmos. Oceans* **2001**, *34*, 327–348.

669
670